Turbine fatigue load prediction from field measurements of waves and turbulence

Hannah Mullings, Samuel Draycott and Tim Stallard

Abstract—**Tidal stream turbines are placed in locations with high flow speeds in order to extract kinetic energy. These flow speeds combined with other environmental factors can lead to complex operating conditions. When assessing turbine loading at alternative locations within a site, most models focus on velocity, shear and turbulence of naturally occurring conditions, with limited analysis including the impact of waves coexisting with currents. Previous studies have analysed the influence of wave conditions from measurements on the loading, through a consideration of the turbine not considered to be operating during large wave conditions. Although tidal conditions are often bi-directional, wave conditions are wind driven, occurring over a range of directions relative to the current; this combination will be investigated in this study. Loading on the turbine components is assessed through an efficient blade element momentum theory method, which is combined with a synthetic turbulence model to provide a time-varying onset flow. This analysis focuses on full-scale site data, which was gathered at the Raz Blanchard, a potential tidal site for multiple deployments, which provides both wave and current conditions over a period of 45 days. The interest in this work is understanding the conditions which contribute to the cyclic loading experienced by a tidal turbine. This work determines the impact of the measured waves, and the way in which they are analysed on the turbulence characteristics in the onset flow, specifically the interaction of waves with current and influence on the loading experienced on the turbine.**

Index Terms—**Directional Waves, Blade Loading, Spatial Variation, Tidal Turbine.**

I. Introduction

THE installation of tidal stream turbines (TST) at suitable sites across the UK has been predicted to contribute by 11% to the energy demand, [1], by being part of the mix of different electricity generators. One of the key factors in the usefulness of including tidal stream energy is the reliable and predictable nature of the resource. Many studies have been performed to determine the most suitable sites around the UK [2] and the World [3]. Most of these studies have been performed using resource models based in shallow water equations, some have been validated using measurement deployments at the sites, such as the work in [4]–[6]. One of the aims of these models is to assess the variation in the ambient flow conditions, to potentially see the impact of those conditions on the energy density and yield from the site. These conditions are important in identifying appropriate sites, but more detail of the unsteady onset flow conditions is needed to determine the loading and fatigue life of the turbine components.

Unsteady conditions are defined by complex characteristics within the onset flow, such as shear, turbulence and waves. These conditions are defined within the Tidal Design Standards [7] as identifiable under 'normal' operating conditions which contribute to the calculation of fatigue. Studies have looked into the impact of measured turbulence conditions at a location on the fatigue of tidal turbines [8] and [9]. Although these conditions are known to influence the cyclic loading, the magnitude of the influence can vary with location, turbine position and with the chosen operating point. Previous studies by the authors focusing on a single tidal site, [10], showed that measurement data showed a variation in turbulence and vertical shear between two locations in a site, and a difference in the loading for a turbine located near-surface to a near-bed device for the same operating point.

The measurement of unsteady site conditions is commonly conducted by an Acoustic Doppler Current Profiler (ADCP), [11] [12] [13], with a set up refined to capture turbulence characteristics and for some cases, wave characteristics. Some studies have looked into determining the magnitude of the Turbulent Kinetic Energy (TKE) using different types of ADCP [13] and by removing the influence of the waves from the TKE using filtering techniques [14], [15]. The site of Raz Blanchard has had numerous measurement campaigns conducted in the recent years due to the highly energetic tidal conditions. These campaigns have been used to study; the spatial variation of conditions in [16] [6], the change in bathymetry and different bed structures on the flow field [17] [18], the characterisation of turbulence [19] [20], and the complex wave-current conditions through 3D modelling [21].

The aim of the analysis presented in this study is to determine the influence of measured environmental conditions on the loading experienced on the blades of a near surface tidal turbine. In order to achieve this, data from a recent deployment of ADCPs in the tidal site, Raz Blanchard, is analysed to define the unsteady

© 2023 European Wave and Tidal Energy Conference. This paper has been subjected to single-blind peer review.

This work was supported by the Tidal Stream Industry Energiser Project (TIGER), co-funded by the European Regional Development Fund through Interreg France Channel Programme, with the lead author supported by this and the Supergen ORE Hub under EPSRC grant no. (EP/S000747/1)

H. Mullings is a Research Fellow at The University of Manchester, Oxford Road, Manchester, M13 9PL (e-mail: hannah.mullings@manchester.ac.uk).

S. Draycott is a Dame Kathleen Ollerenshaw Fellow at The University of Manchester, Oxford Road, Manchester, M13 9PL (e-mail: samuel.draycott@manchester.ac.uk).

T. Stallard is Professor of Offshore and Renewable Energy Engineering at The University of Manchester, Oxford Road, Manchester, M13 9PL (e-mail: tim.stallard@manchester.ac.uk).

Digital Object Identifier:
https://doi.org/10.36688/ewtec-2023-paper-390

operating conditions. These conditions comprise of turbulence, waves and shear. In order to determine the influence of the waves and turbulence individually, the measured wave conditions will be used to identify the velocity contributions purely due to each condition. This is done using the measured directional spectra to determine the expected components of velocity and alignment of these components them with the corresponding current beam measurements. Subsequently, an efficient blade element model combined with a synthetic turbulence inflow, and the range of measured conditions will provide predicted loading on the turbine. A single design condition is presented to highlight the impact unsteady onset conditions can have on an operating point considered to have the same power output.

II. Model Set Up

A. Site Conditions

This work focuses on the conditions at one of the sites studied within the Interreg TIGER project, Raz Blanchard, which is located between the coasts of France and the Channel Island of Alderney. Understanding the conditions at this site is of considerable importance to tidal energy developers, as two developers, Normandie Hydrolienne and Hydroquest, currently have plans in place to deploy arrays of devices. The field measurements used here were gathered as part of the project using a Nortek Signature500 ADCP, located in a depth of approximately 48 m.. From a period of time in early 2022 (January - March), both current and waves were measured with this device, with the currents measured with a sampling frequency of 2 Hz and the waves measured using the burst setting in 30 minute intervals. For consistency with design standards the current conditions will be time-averaged into 10 minute 'bins' in order to determine the quasi-steady onset flow conditions, a turbine of diameter = 18 m and hub depth = -15 m, are considered. With comparison to the measured wave conditions the wave will be considered as stationary over the 30 minute period and therefore applied appropriately to the corresponding 10 minute current conditions as required.

The current conditions are measured as vertical profiles across four beams of the ADCP. These beam velocities are used to define the current direction and magnitude, as well as the vertical, transverse and longitudinal velocities. With a vertical bin size of 1 m, allowing a series of velocities to be measured across the depth of the rotor. The focus in this study is on the load predictions due to waves and turbulence, and so a turbine positioned near the water surface is chosen. The methodology which will be presented in this paper will be applied to one quasi-steady operating point defined by the 10 minute averaged onset flow conditions. The chosen operating point is for a turbine operating within a flow speed range of 2.2 - 2.4 m/s, where a 0.2 m/s flow speed range is chosen to align with the recommendations in the Tidal Design Standards [7]. The flow speed range is defined using the disk averaged velocity calculated as a power weighted disk average, following the work in [22] and [23]. This velocity is calculated from the measurements at different vertical positions down the rotor plane, then averaged over the rotor area using Equation 1.

$$U_{DA} = \left[\frac{1}{A_D} \sum_{i=1}^{n} U_i^3(z) A_i \right]^{1/3} \quad (1)$$

Where A_D is the rotor area, $U_i(z)$ is the velocity at each vertical velocity bin, which is cubed for the power-weighted average and A_i is the strip wise area of each bin.

Using this equation the disk averaged velocities have been calculated for every 10 minute average, across the time period of wave and current measurements from the ADCP. These velocities are given in Figure 1, with the range of samples in the 2.2 - 2.4 m/s flow speed bin highlighted. Across this time period the number of samples is 703 for both flood and ebb which represents just over 6.5% of the total number of cases.

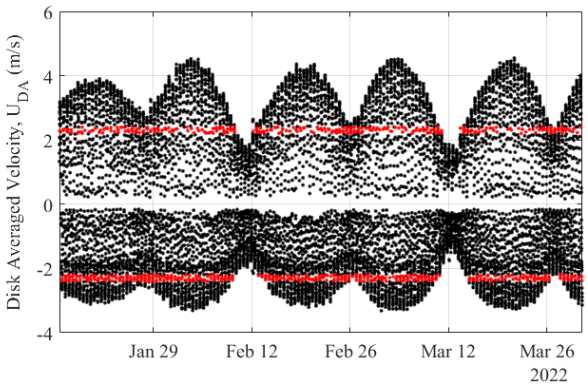

Fig. 1. Calculated disk averaged velocities for a turbine located near surface using the ADCP field measurements, black markers across time period showing all disk averaged velocities and red markers highlighting the chosen sample disk averaged velocities (2.2-2.4 m/s).

For each of the chosen cases the measured velocities which are sampled at 2 Hz, provide a level of detail to determine the turbulence intensity (TI), which is calculated using Equation 2.

$$TI = \frac{u'}{\bar{u}} \quad (2)$$

Where $\bar{u}$ is the mean velocity and u' is the root-mean-square of the velocity fluctuations. This calculation when applied directly to measurements from a current profiler, allows for the description of turbulence to include all conditions which impact the fluctuations of velocity over the sample period. The intensity values are calculated across the rotor area using the disk averaged approach which was applied to the velocities, so the depth variation of calculated intensity from Equation 2 is accounted for. The values of intensity calculated from the measurements are shown in Figure 2 across the range of calculated disk averaged velocities. The intensities are determined for both the ebb and flood tides, with the mean and range of intensity at each binned U_{DA} presented in Figure 2 as the markers and band of colour. For the flow speed range of interest

(2.2-2.4 m/s) the mean TI for the flood tide is greater at 11.9% than for the ebb tide at 11.1%. The range around the mean for the flood tide is between 10.3% to 13.2% and for the ebb tide is between 9.5% to a maximum of 12.7%. So although the ebb tide has a lower mean value the range of intensities vary by around 3% for both tides.

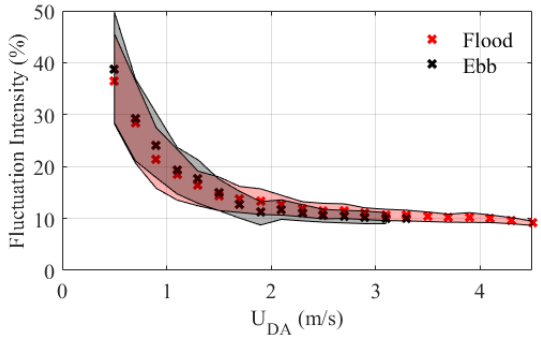

Fig. 2. Variation of the disk averaged fluctuation intensity for the flood and ebb tides across range of disk averaged velocities, with the mean value shown by (x) at each binned flow speed. The full range of intensities at each flow speed is also shown by the shaded areas, with the flood tide (red) and ebb tide (grey).

The overall trend for the disk averaged intensities and flow speed follows the measurements and calculations for other tidal sites, [24]. The values calculated also correspond to data and results for the Raz Blanchard site as shown in [4] and [6]. This variation of intensity for the specific flow speed range, is used when defining the onset flow field that a turbine will experience. In addition, the vertical shear measured at a site is of importance when determining the cyclic loads which contribute to fatigue. As the ADCP is bed mounted, facing the surface it measures the vertical profile of the velocities, used to determine the disk averaged velocity. The same measurements are used to define the vertical shear experienced at the ADCP location. Figure 3 is included to show the variation of shear for each binned disk average velocity. Across this range a more severe shear is found at the higher disk averaged flow speeds, which are not present in the ebb tide.

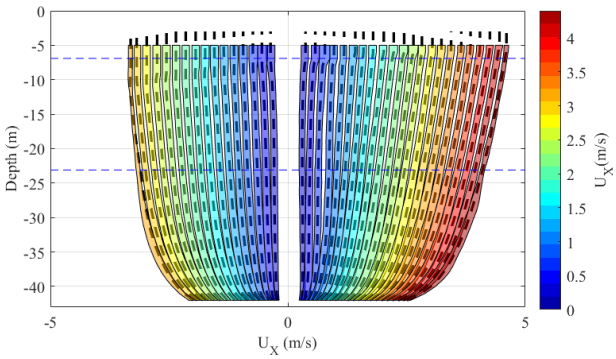

Fig. 3. Variation in current velocity with depth for all 10 minute samples in the measurement period, binned using the disk averaged velocities for a turbine located near the surface. Turbine position is shown by the blue dashed lines.

In this work the range of shear profiles for the flow speed of interest, are incorporated into the flow fields which are used to determine the turbine loading. Further details on the set up of the onset flow field are given in Section II-B. The variation with depth across the disk area is shown in Figure 4. This figure shows the mean and range in the variation across the sample cases for the flood and ebb tides. This has been compared to a 1/7th power law shear profile for the mid point velocity of 2.3 m/s. For the ebb tide the curvature of the power law profile closely follows the mean profile, whereas with the flood tide the mean profile has a steeper gradient than the chosen power law profile.

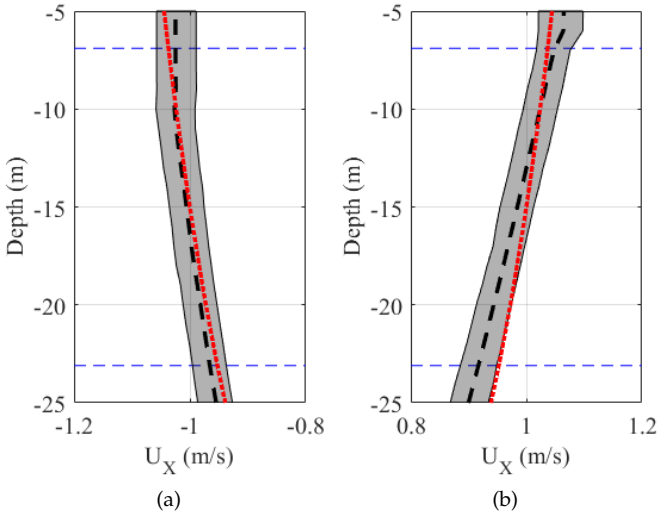

Fig. 4. Variation in current velocity with depth over the disk area for the chosen binned disk average velocity of 2.2 - 2.4 m/s. Mean variation shown by the black dashed line, range of profiles shown by the grey shading, 1/7th power law profile shown in red.

Using the conditions measured by an ADCP, the variation in velocity within each 10 minute sample includes the impact of waves at the free surface which have been occurring during the measurement campaign. The data collected as part of this project includes the wave defining characteristics of time period and significant height for each sample. The occurrence of the significant wave height and peak period for the chosen sample of velocities are given in Figure 5. These occurrences have been separated into whether they occur in the flood or ebb tides. For both tides there seems to be a spread between 0.5-5 m, but with the ebb tide having a higher percentage of occurrence below 1 m. With the flood tide the greatest occurrence of wave height is between 1-2 m.

The wave data collected also goes a step further and can provide more detailed data using this particular measurement device, the Nortek Signature500, which has the use of a fifth beam and therefore acoustic surface tracking. This tracking enables the determination of the directional spectra of the waves measured for each burst. The directional spectra shows the spreading of the wave field with both frequency and direction. This data will also be used to define the impact of the waves on the original velocity measurements from the

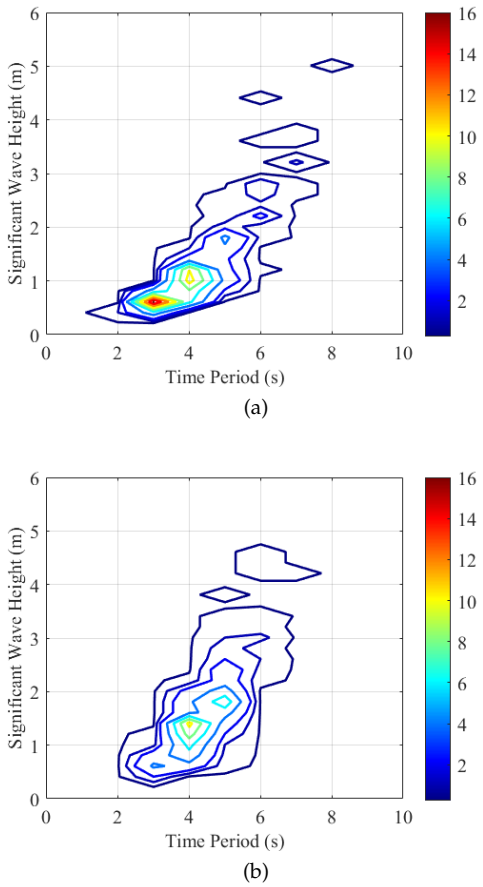

Fig. 5. Percentage occurrence of wave period with significant wave height for the chosen sample of flow speeds for both (a) the ebb tide and (b) the flood tide

ADCP beams. Further discussion on how this will be implemented is given in Section III.

B. Onset Flow Field

In order to determine the loading on a turbine using the onset conditions mentioned in the previous section the flow field needs to be simulated. This can be done using computational fluid dynamics software, with Reynolds Averaged Navier Stokes (RANS), to simulate the turbulence properties, [25]–[28], In order to provide more detail of the conditions, some cases use Large Eddy Simulations (LES) to simulate the turbulent conditions including the influence of bed structures and other turbines within a simulation, [29], [30]. The disadvantage of these methods is the computational expense to set up a domain large enough to consider a full scale turbine, running for a design case of at least 10 minutes, which corresponds to one set up condition. In this case multiple onset flow cases want to be investigated efficiently, therefore a statistical turbulence generation method is used, the Von Kármán method. This method for defining turbulence has been used in defining onset conditions to wind turbines, fully incorporated into commercial software Bladed from DNV-GL, and subsequently applied to the inflow for tidal turbines, [31], [10].

This method is a random statistical approach to model combined stochastic velocity spectra, where auto-spectral density functions are used to describe real atmospheric turbulence. This creates a 3D grid of synthetic turbulence over a time period which is propagated using Taylor's frozen turbulence hypothesis, [32]. The turbulence characteristics of the onset flow field are defined using the intensity determined from the site conditions and the turbulence lengthscale of 21 m which is kept consistent for the conditions modelled in this work. The set up of the onset flow field then follows Equation 3, where the unsteady time varying characteristics of the flow can be defined.

$$u = \overline{u} + \tilde{u} + u' \tag{3}$$

Where the overall onset flow, u, is created by a mean value, $\overline{u}$, a fluctuating component, u' and a periodic component, $\tilde{u}$.

With the magnitude of the fluctuating component defined by the turbulence, and the periodic component defined by any shear profiles. The influence of the waves can impact both the fluctuating and periodic components, depending on the way they are modelled and included in the flow field. In this work they will be considered to impact the fluctuating component only.

C. Modelling the Turbine

To determine the influence of the conditions on a tidal turbine a full scale tidal turbine needs to be modelled. In this case the Alstom Energy's DEEP-Gen IV 1 MW tidal turbine has been chosen, and can also be referred to as the TGL 1 MW device .This device is chosen due to the availability of geometry data, ([33], [34]). This turbine has three blades and a diameter of 18 m and is located with a clearance of at least 6 m between the blade tip and the surface. Current design of tidal turbines have larger diameters and produce more power, [35], but the geometry detail required for modelling is not publicly available. The variation in disk averaged velocity determined from the site conditions leads to varying angular speed of the turbine to allow a constant tip-speed-ratio (TSR) for all cases to be achieved.

The geometry of the turbine is incorporated into each simulation case through the use of a blade element momentum theory model (BEM). The blades are defined by a series of points 'elements' along the radius. This number can vary depending on the geometry of the blade. A basic overview of the method is provided in this section for an arbitrary number of elements defined by $'N'$. The relative velocity (U_{rel}) at each element is desired and depends upon the onset flow and the rotational speed of the turbine, ω_t, given by Equation 4. With the inflow angle to the blade element defined by Equation 5.

$$\delta U_{rel}(t) = \sqrt{U_X^2 + (\omega_t r - U_\Theta)^2)} \tag{4}$$

$$\delta\phi(t) = sin^{-1}\frac{U_X(t)}{U_{rel}(t)} \tag{5}$$

Where U_{rel} is the relative velocity to the blade which incorporates the longitudinal velocity, U_X is the

stream-wise onset velocity which includes axial induction, a through $U_X = U_0(1-a)$ and the components in the tangential direction, U_Θ with the angular velocity ω and each radius r.

In addition to the velocities on the blade the forces also need to be resolved. In order to determine these, the lift and drag polars are required, these depend upon the chosen geometry of the blade. The lift and drag force on each blade segment vary according to Equations 6-7.

$$\delta L(t) = \frac{1}{2} B\rho c (U_{rel})^2 C_L \delta r \tag{6}$$

$$\delta D(t) = \frac{1}{2} B\rho c (U_{rel})^2 C_D \delta r \tag{7}$$

Where c is the chord length, δr is the radial width of the blade segment, B is the number of blades, ρ is the fluid density, C_L and C_D correspond to the lift and drag coefficients respectively.

Using the calculated lift and drag forces for each blade the axial (F_a) and tangential (F_t) forces along each blade are calculated using Equations 8-9.

$$\delta F_a(t) = \delta L(t)\cos(\phi(t)) + \delta D(t)\sin(\phi(t)) \tag{8}$$

$$\delta F_t(t) = \delta L(t)\sin(\phi(t)) - \delta D(t)\cos(\phi(t)) \tag{9}$$

The axial force (F_a) on each segment of the blade leads to the calculation of root bending moment as well as rotor thrust. These results can be used to establish the respective load spectra and hence determine the load cycles enabling the fatigue loads to be predicted for the blades and rotor. More details on the use of this model are found in [36], [37].

D. Quantifying the Fatigue Loads

The time varying loads which are determined from the BEM model are then used to calculate the fatigue loads. In this study the fatigue loads are quantified through the Damage Equivalent Load (DEL) value. This load is determined using Equation 10, which defines a single magnitude load repeating at a single frequency which would cause the same damage as the varying initial load.

$$L_m = \left(\frac{\sum_i n_i L_i^m}{fT} \right)^{1/m} \tag{10}$$

Where n_i is the number of cycles at each binned load magnitude, m is the material gradient, f is the repetition frequency, T is the time sample length, L_i is the load bin, and L_m is the damage equivalent load for a given material gradient.

The load cycles are calculated using Rainflow Cycle Counting method ([38]), which allows cycles of varying magnitude to be counted. Fatigue loads on offshore components have been calculated using this method in ([39], [40]). The number of calculated load cycles and magnitude of the cycles can be used to determine the lifetime of a component using Palmgren Miner's Rule when modelling over the full range of conditions and aggregating the loads.

III. Determining the Influence of Waves

This section describes the methodology to determine the influence the waves have on the measured kinematics. Three different approaches will be used. The first case utilises the standard wave characteristics, the significant wave height (H_S) and the time period (T_P). These parameters can be obtained from the ADCP measurements, regardless of whether or not the device has a fifth beam for surface tracking. These conditions will be combined with an assumed spectral shape and a synthetic turbulent inflow in order to determine the impact waves have on the onset flow conditions and therefore the loading of the turbine. The assumed spectra which has been chosen here is based on the Pierson-Moscovitz spectrum (S_{PM}) which is defined by Equation 11.

$$S_{PM}(f) = \left(\frac{5}{4} \frac{f_P^4}{f^4} \right) e^{-\left(\frac{5}{4} \frac{f_P^4}{f^4} \right)} \tag{11}$$

Where f_P is the peak frequency defined by the time period Tp, with the spectra defined across the frequencies by f. The amplitude, a, across this frequency range is defined by Equation 12.

$$a(f) = \sqrt{2 S_{PM}(f) df} \tag{12}$$

The second case will consider the measured Hs and Tp, as well as the spectra determined from the measurements, and will be applied to the turbulent flow field in the same way as the modelled spectra. Figure 6 shows the energy spectra for both the modelled and measured data for these cases. This figure highlights the difference in the predicted modelled spectra, a similar trend is observed, where the peak frequencies are located. However, visually it can be seen that there is more spectral energy at the chosen peak frequencies for some of the cases with the modelled spectra. With the model predicting the spectral energy to within 3.0% for the flood tide cases and 2.6% for the ebb tide, when compared to the measurement data. The impact of the chosen spectra on the loading will be observed in a later section.

The third case focuses on the use of the directional spectra measured by the ADCP. The ADCP measures the velocity along each beam, in order to calculate the current speed and direction, post-processing takes place to extract the velocities respective of the earth co-ordinate system, East, North and Up (ENU), or in the cartesian co-ordinate system of X, Y and Z, with respect to the orientation of the ADCP, with beam 1 aligning with X. In this case the mean current speed and direction have been used in the analysis for the disk averaged velocities and wave comparisons. Figure 7 is included to show the variation in mean direction from the current and wave data obtained by the ADCP. Both of these sets of values have been plotted with respect to the disk averaged velocity of interest (2.2-2.4 m/s). The dominant ebb and flood tide directions are clearly shown in Figure 7(a), with the flood tide having a dominant direction between 5^o and 15^o and the ebb tide between 195^o and 210^o, which is consistent

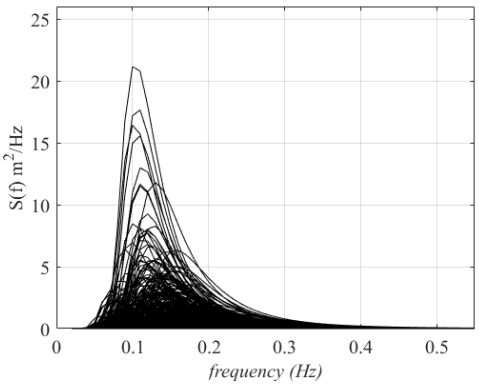

(a) Modelled

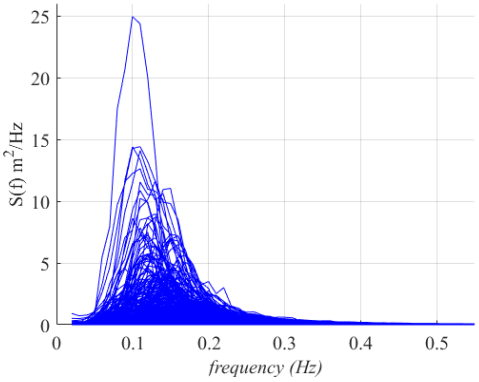

(b) Measured

Fig. 6. Spectral Energy from the measured waves at the site for (a) Pierson-Moscovitz spectra using measured Hs and Tp and (b) Measured energy spectra.

with the measurements reported from the THYMOTE project in Raz Blanchard by [17], [41]. With the waves caused predominately by wind, as mentioned previously the tidal site of Raz Blanchard has numerous characteristics which make for a complex environment. The measurements taken here show a range of wave directions, with a dominant portion between 200^o to 300^o, in a westerly direction, which corresponds to the measurements reported in [21]. With 82% of samples during the flood tide occurring within this range of direction and 71% in the ebb tide. During the flood tide, the measured wave direction coincides with the dominant current flow direction for less than 3% of samples within the measured time period for the chosen disk average velocity range. During the ebb tide, the measured wave direction coincides with the current direction for 0.25% of the samples within the time period. However, during the ebb tide 5.2% of the measured wave direction coincides with the direction of the flood tide and therefore causing the waves to be fully opposing the current.

The directional spread of the measured wave conditions is used to determine the influence on the original measured ADCP velocities. The use of the directional spectrum provides the most information with regard to the direction and spread of the wave within each 30 minute sample. For each case the directional spectrum can be split into components for each frequency and direction 'bin'. For each bin the amplitude is calculated

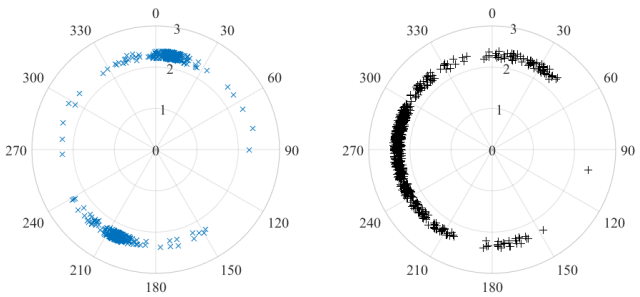

(a) (b)

Fig. 7. Polar plots showing (a) the dominant mean current direction and the mean wave direction (b) from the ADCP measurements.

using an updated Equation 12 as Equation 13.

$$a_s(f,\theta) = \sqrt{2S(f,\theta)df d\theta} \tag{13}$$

Where a_s is the amplitude over each frequency and direction and $S(f,\theta)$ defines the spectra energy with both frequency and direction. These calculated amplitudes are then used to determine the wavenumber, k, for each frequency and direction component using Equation 14.

$$\omega_a = \sqrt{\omega_r - kU} = \sqrt{gk\tanh(kd)} \tag{14}$$

Where ω_a is the absolute angular frequency, ω_r is the angular frequency relative to the current and U is the effective current with respect the angle between the mean wave and current directions. These wavenumbers, k, are calculated to allow for the wave induced velocity components to be identified, again with both frequency and direction, through Equations 15 and 16.

$$U_w = \left(\frac{gka_s}{\omega_r}\right)\left(\frac{\cosh(k(z+d))}{\cosh(kd)}\right) \tag{15}$$

$$W_w = \left(\frac{igka_s}{\omega_r}\right)\left(\frac{\sinh(k(z+d))}{\cosh(k(d)}\right) \tag{16}$$

Where the components of the horizontal wave velocity with direction are defined by $U_U(f,\theta,h) = U_w(f,\theta,h)cos(\theta)$ and $V_U(f,\theta,h) = U_w(f,\theta,h)sin(\theta)$. With the wavenumber and amplitude being defined by $k(f,\theta)$ and $a_s(f,\theta)$ respectively and the depth by, $z(h)$, where θ is the angle with respect to the ADCP frame of reference. Each wave-induced velocity component, (U,V,W) is then used to determine the component velocity for each beam with respect to the ADCP. This is done using a transformation matrix and the heading, pitch and roll data recorded from the ADCP. By determining the wave-induced velocity components for each beam within the frequency domain the amplitudes are then removed from the Fourier transform of the amplitudes of the measured beam velocities. The original phase of the signal is then kept to return these velocities into the time domain for analysis as an inflow condition to the model. Initially the impact on the shear and turbulence was examined, with the shear having a minimal impact across the disk. However, the variation across the disk due to turbulence has reduced

with the mean disk averaged turbulence for the flood tide at 4.1% and for the ebb tide at 4.0%. There is less difference between the two tidal periods than the previously calculated value from the measurements, they are also at least 7.1% lower. As observed with the new calculations of shear, the disk averaged velocity values have not differed from the 2.2-2.4 m/s range and therefore the difference in turbulence intensity is due to the variance of velocity with depth.

IV. Turbine Loading

A. Direct from Turbulent Conditions

Initial turbine blade loading results for a single design condition (2.2 -2.4 m/s) using the ADCP current data are determined here, where the blade loading is quantified by the flap-wise root bending moment.

The damage equivalent loads are determined as an aggregated value across the time varying loads for all samples. Figure 8 shows the variation in DEL for the flood and ebb tides depending on the turbulence intensity value used in the simulations. There is an 11.6% reduction in aggregated DEL across the range of samples for the ebb tide when compared to the flood tide using the measured turbulence intensity for each case. The difference between the two tides reduces to less than 1% when the mean turbulence intensity is used to define the onset flow field and subsequent loading is calculated. The loads calculated with the mean turbulence intensity are 24.6% and 15.3% lower than those determined using the measured turbulence intensity for the flood and ebb tides respectively.

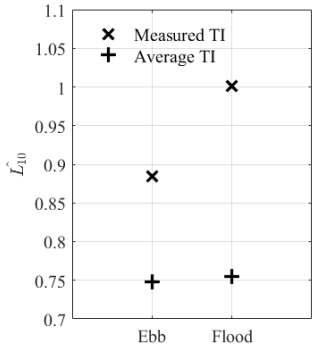

Fig. 8. Normalised damage equivalent loads, using both the measured turbulence intensity across all samples, and the average turbulence intensity. For both the flood and ebb tides.

These results use the measurement values for turbulence and shear which will include any potential influence from waves. Due to the wave data acquired in this project, numerous cases have been set up which look at the contribution waves can make on these parameters, especially the turbulence.

B. Considering Measured Wave Conditions

Using the methods outlined in Section III the waves can be identified and defined. Firstly, the influence of the waves on the conditions has been used to redefine the flow field set up, so new shear profiles and turbulence intensities have been included. The results have been included in Figure 9 in comparison with the original results. The main influence on these results is the reduction in turbulence intensity, as previously reported to have decreased by 7%. This has lead to a reduction on DELs predicted from the varying turbulence 31% for the ebb tide and 42% for the flood tide. When a mean turbulence intensity value is used the DELs have reduced by 40% for the ebb tide and 51% for the mean. The mean loads however do not experience the same reduction, showing the impact the fluctuations have on the load cycles and hence the damage equivalent load calculation.

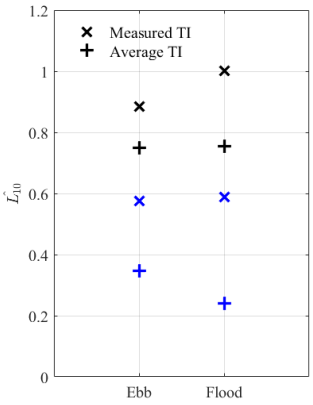

Fig. 9. Normalised damage equivalent loads for the case with wave conditions removed from the beam velocities, shown in blue, original loads shown in black.

In addition to using the directional spectra, to determine the magnitude of the wave contribution to the onset flow field, the measured and modelled unidirectional spectra have also been used to examine the influence of waves with shear and a steady onset flow. The damage equivalent load results for the measured and modelled spectra, combined with a steady flow field and the measured shear are shown in Figure 10. Although the mean root bending moments for both the ebb and flood tide are 3% greater than the original case using the fully measured conditions the predicted DELs are considerably lower. This highlights the influence of the turbulence the impact that both waves and turbulence can have on the predicted DELs. Figure 10 also shows the variation in predicted DEL using both the measured and modelled spectra. With less than 0.1% difference for the predicted DEL in the flood tide, and a 1.5% decrease in the ebb tide for the measured case. For this prediction of DEL the use of the measured wave spectra does not contribute enough of an overall impact and therefore Hs and Tp obtained on their own could be suitable. Although these predictions were based upon the original measured conditions have the influence of the waves removed, before being included from the wave spectra.

It is important to fully understand the variation in site conditions and their impact on the loading for fatigue calculations on a tidal turbine. In this work site measurements have shown a distinct difference between the mean current directions and the waves. The influence of these conditions can be calculated by

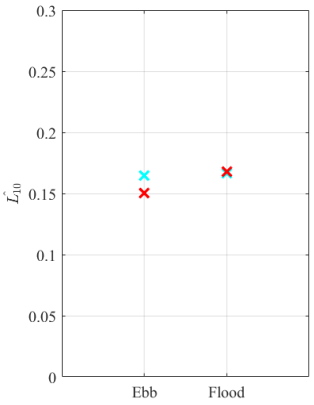

Fig. 10. Normalised damage equivalent loads for the case with only waves applied as the original measured unidirectional spectra in red and a modelled spectra in cyan.

extracting from the measured beam velocities, but further investigation is necessary to fully understand the impact on aggregated loading across multiple design conditions.

V. Conclusion

This work has examined a method to remove the influence of waves from measured current data with directional spectra provided. For a turbine located near-surface, measured turbulence intensity reduces from 11% to 4% when this approach is applied. This difference of turbulence intensity impacts the predicted damage equivalent loads, with the DEL obtained on the basis that all measured fluctuations represent turbulence reduced by a third when the kinematics associated with measured waves are considered separately. The DEL predicted due to the flow and waves only, neglecting turbulence, is approximately half of this difference. This indicates that consideration of all measured fluctuations as turbulent may lead to higher turbulence intensity, and also fatigue load, than obtained when both waves and turbulence are considered individually. The extent to which waves influence flow-parameters obtained from measurements and the influence on the magnitude of predicted loading highlights the importance of a full understanding of the combination of unsteady flow conditions occurring at tidal stream operating locations. In this study a single operating point is considered based on conditions measured during a winter period (Jan-Mar). Ongoing analysis considers further the range of operating conditions, longer-term variation of occurrence and the impact of strategies such as pitch control on load mitigation in turbulence, waves and coexisting of these conditions.

References

[1] D. Coles, A. Angeloudis, D. Greaves, G. Hastie, M. Lewis, L. MacKie, J. McNaughton, J. Miles, S. Neill, M. Piggott, D. Risch, B. Scott, C. Sparling, T. Stallard, P. Thies, S. Walker, D. White, R. Willden, and B. Williamson, "A review of the UK and British Channel Islands practical tidal stream energy resource," *Proceedings of the Royal Society A: Mathematical, Physical and Engineering Sciences*, vol. 477, no. 2255, 2021.

[2] M. Lewis, S. P. Neill, P. E. Robins, and M. R. Hashemi, "Resource assessment for future generations of tidal-stream energy arrays," *Energy*, vol. 83, pp. 403–415, 2015. [Online]. Available: http://dx.doi.org/10.1016/j.energy.2015.02.038

[3] C. R. Vogel, D. T. Taira, B. S. Carmo, G. R. S. Assi, R. H. J. Willden, and J. R. Meneghini, "Prospects for Tidal Stream Energy in the UK and South America: A Review of Challenges and Opportunities," *Polytechnica*, vol. 2, no. 1-2, pp. 97–109, 2019.

[4] A. C. Bourgoin, S. S. Guillou, J. Thiébot, and R. Ata, "Turbulence characterization at a tidal energy site using large-eddy simulations: case of the Alderney Race," *Philosophical transactions. Series A, Mathematical, physical, and engineering sciences*, vol. 378, no. 2178, p. 20190499, 2020.

[5] J. Thiébot, D. S. Coles, A. C. Bennis, N. Guillou, S. Neill, S. Guillou, and M. Piggott, "Numerical modelling of hydrodynamics and tidal energy extraction in the Alderney Race: a review," *Philosophical transactions. Series A, Mathematical, physical, and engineering sciences*, vol. 378, no. 2178, p. 20190498, 2020.

[6] S. Guillou, A. Bourgoin, J. Thiébot, and R. Ata, "On the spatial variability of the flow characteristics at a Tidal energy site : Case of the Raz Blanchard," in *Proceedings of the 14th European Wave and Tidal Energy Conference, 5-9th Sept 2021, Plymouth, UK*, 2021, pp. 1–8.

[7] DNV-GL, "Standard Tidal Turbines (DNVGL-ST-0164)," Tech. Rep. October, 2015.

[8] I. Milne, A. Day, R. Sharma, and R. Flay, "Blade loading on tidal turbines for uniform unsteady flow," *Renewable Energy*, vol. 77, pp. 338–350, 2015. [Online]. Available: http://linkinghub.elsevier.com/retrieve/pii/S0960148114008556

[9] M. Thiébaut, J. F. Filipot, C. Maisondieu, G. Damblans, C. Jochum, L. F. Kilcher, and S. Guillou, "Characterization of the vertical evolution of the three-dimensional turbulence for fatigue design of tidal turbines," *Philosophical transactions. Series A, Mathematical, physical, and engineering sciences*, vol. 378, no. 2178, p. 20190495, 2020.

[10] H. Mullings and T. Stallard, "Assessment of dependency of unsteady onset flow and resultant tidal turbine fatigue loads on measurement position at a tidal site," *Energies*, vol. 14, no. 17, pp. 1–13, 2021.

[11] M. Guerra and J. Thomson, "Turbulence measurements from five-beam acoustic doppler current profilers," *Journal of Atmospheric and Oceanic Technology*, vol. 34, no. 6, pp. 1267–1284, 2017.

[12] E. Osalusi, J. Side, and R. Harris, "Structure of turbulent flow in EMEC's tidal energy test site," *International Communications in Heat and Mass Transfer*, vol. 36, no. 5, pp. 422–431, 2009. [Online]. Available: http://dx.doi.org/10.1016/j.icheatmasstransfer.2009.02.010

[13] M. Togneri, D. Jones, S. Neill, M. Lewis, S. Ward, M. Piano, and I. Masters, "Comparison of 4- and 5-beam acoustic Doppler current profiler configurations for measurement of turbulent kinetic energy," *Energy Procedia*, vol. 125, pp. 260–267, 2017. [Online]. Available: http://dx.doi.org/10.1016/j.egypro.2017.08.170

[14] L. Perez, R. Cossu, A. Grinham, and I. Penesis, "Evaluation of wave-turbulence decomposition methods applied to experimental wave and grid-generated turbulence data," *Ocean Engineering*, vol. 218, no. May, p. 108186, 2020. [Online]. Available: https://doi.org/10.1016/j.oceaneng.2020.108186

[15] M. Togneri, I. Masters, and I. Fairley, "Wave-turbulence separation at a tidal energy site with empirical orthogonal function analysis," *Ocean Engineering*, vol. 237, no. June, p. 109523, 2021. [Online]. Available: https://doi.org/10.1016/j.oceaneng.2021.109523

[16] L. Furgerot, A. Sentchev, P. Bailly du Bois, G. Lopez, M. Morillon, E. Poizot, Y. Méar, and A. C. Bennis, "One year of measurements in Alderney Race: preliminary results from database analysis," *Philosophical transactions. Series A, Mathematical, physical, and engineering sciences*, vol. 378, no. 2178, p. 20190625, 2020.

[17] P. Mercier, M. Grondeau, S. Guillou, J. Thiébot, and E. Poizot, "Numerical study of the turbulent eddies generated by the seabed roughness. Case study at a tidal power site," *Applied Ocean Research*, vol. 97, no. March, p. 102082, 2020. [Online]. Available: https://doi.org/10.1016/j.apor.2020.102082

[18] P. Mercier and S. Guillou, "The impact of the seabed morphology on turbulence generation in a strong tidal stream," *Physics of Fluids*, vol. 33, no. 5, 2021.

[19] M. Thiébaut, J. F. Filipot, C. Maisondieu, G. Damblans, R. Duarte, E. Droniou, N. Chaplain, and S. Guillou, "A comprehensive assessment of turbulence at a tidal-stream energy site influenced by wind-generated ocean waves," *Energy*, vol. 191, jan 2020.

[20] P. Mercier, S. S. Guillou, J. Thiébot, and E. Poizot, "Turbulence characterisation during ebbing and flooding tides in the Raz Blanchard with large eddy simulations," in *Proceedings of the 14th European Wave and Tidal Energy Conference, 5-9th Sept 2021, Plymouth, UK*, 2021.

[21] A. C. Bennis, L. Furgerot, P. Bailly Du Bois, F. Dumas, T. Odaka, C. Lathuilière, and J. F. Filipot, "Numerical modelling of three-dimensional wave-current interactions in complex environment: Application to Alderney Race," *Applied Ocean Research*, vol. 95, no. January, p. 102021, 2020. [Online]. Available: https://doi.org/10.1016/j.apor.2019.102021

[22] J. McNaughton, S. Harper, R. Sinclair, and B. Sellar, "Measuring and Modelling the Power Curve of a Commercial-Scale Tidal Turbine," in *Proceedings of 11th European Wave and Tidal Energy Conference, Nantes, France*, vol. 1, 2015, pp. 1–9.

[23] IEC, "Power Performance Assessment of Electricity Producing Tidal Energy Converters, IEC 62600-200," Tech. Rep., 2012.

[24] H. R. Mullings and T. Stallard, "Impact of spatially varying flow conditions on the prediction of fatigue loads of a tidal turbine," *International Marine Energy Journal*, vol. 5, no. 1, pp. 103–111, 2022.

[25] a. Olczak, T. Stallard, T. Feng, and P. K. Stansby, "Comparison of a RANS blade element model for tidal turbine arrays with laboratory scale measurements of wake velocity and rotor thrust," *Journal of Fluids and Structures*, vol. 64, pp. 87–106, 2016. [Online]. Available: http://dx.doi.org/10.1016/j.jfluidstructs.2016.04.001

[26] J. McNaughton, S. Rolfo, D. Apsley, I. Afgan, P. Stansby, and T. Stallard, "CFD prediction of turbulent flow on an experimental tidal stream turbine using RANS modelling," *1st Asian Wave and Tidal Conference Series*, 2012.

[27] I. Afgan, J. McNaughton, S. Rolfo, D. Apsley, T. Stallard, and P. Stansby, "Turbulent flow and loading on a tidal stream turbine by LES and RANS," *International Journal of Heat and Fluid Flow*, vol. 43, pp. 96–108, 2013. [Online]. Available: http://linkinghub.elsevier.com/retrieve/pii/S0142727X13000672

[28] D. D. Apsley, T. Stallard, and P. K. Stansby, "Actuator-line CFD modelling of tidal-stream turbines in arrays," *Journal of Ocean Engineering and Marine Energy*, 2018. [Online]. Available: http://link.springer.com/10.1007/s40722-018-0120-3

[29] P. Ouro, M. Harrold, T. Stoesser, and P. Bromley, "Hydrodynamic loadings on a horizontal axis tidal turbine prototype," *Journal of Fluids and Structures*, vol. 71, pp. 78–95, 2017. [Online]. Available: http://dx.doi.org/10.1016/j.jfluidstructs.2017.03.009

[30] M. Grondeau, J. C. Poirier, S. Guillou, Y. Mear, P. Mercier, and E. Poizot, "Modelling the wake of a tidal turbine with upstream turbulence : LBM-LES versus," in *Proceedings of the 13th European Wave and Tidal Energy Conference*, vol. 1, no. 2, 2019, pp. 1–7.

[31] I. a. Milne, R. N. Sharma, R. G. J. Flay, and S. Bickerton, "The Role of Onset Turbulence on Tidal Turbine Blade Loads," in *17th Australasian Fluid Mechanics Conference Auckland New Zealand 59 December 2010*, no. December, 2010, pp. 1–8.

[32] G. I. Taylor, "Turbulence in a contracting stream," *Z.a.M.M*, vol. 15, no. 1-2, pp. 91–96, 1935.

[33] G. Scarlett, "Unsteady Hydrodynamics of Tidal Turbine Blades," Ph.D. dissertation, 2019.

[34] G. I. Gretton, "PerAWAT WG3 WP5 D1: Development of a computational fluid dynamics model for an open-centre tidal current turbine," Tech. Rep. WG3 WP5 D1, 2011.

[35] Simec Atlantis, "The Meygen Project," 2018. [Online]. Available: https://simecatlantis.com/projects/meygen/

[36] H. Mullings and T. Stallard, "Analysis of tidal turbine blade loading due to blade scale flow," *Journal of Fluids and Structures*, vol. 114, p. 103698, 2022. [Online]. Available: https://doi.org/10.1016/j.jfluidstructs.2022.103698

[37] E. Mackay, J. Hardwick, D. Coles, P. Mercier, S. Guillou, G. Pinon, E. Mackay, M. Sedrati, P. Thies, E. Mackay, H. Mullings, T. Stallard, M. Campssantamasas, and P. Thies, "Consolidated Report on Site and Turbine Modelling," Tech. Rep., 2023.

[38] S. D. Downing and D. F. Socie, "Simple rainflow counting algorithms," *International Journal of Fatigue*, vol. 4, no. 1, pp. 31–40, 1982.

[39] S. D. Weller, P. R. Thies, T. Gordelier, and L. Johanning, "Reducing Reliability Uncertainties for Marine Renewable Energy," *Journal of Marine Science and Engineering*, vol. 3, pp. 1349–1361, 2015.

[40] S. G. Parkinson and W. J. Collier, "Model validation of hydrodynamic loads and performance of a full-scale tidal turbine using Tidal Bladed," *International Journal of Marine Energy*, vol. 16, pp. 279–297, 2016. [Online]. Available: http://dx.doi.org/10.1016/j.ijome.2016.08.001

[41] P. Mercier, S. Guillou, and E. Poizot, "High resolution large eddy simulation for tidal site turbulence characterisation," in *13th European Wave and Tidal Energy Conference 1-6 September 2019, Naples, Italy*, 2019, pp. 1–7.